# A high-resolution integrated model of the National Ignition Campaign cryogenic layered experiments

O. S. Jones, C. J. Cerjan, M. M. Marinak, J. L. Milovich, H. F. Robey et al.

Citation: Phys. Plasmas **19**, 056315 (2012); doi: 10.1063/1.4718595
View online: http://dx.doi.org/10.1063/1.4718595
View Table of Contents: http://pop.aip.org/resource/1/PHPAEN/v19/i5
Published by the American Institute of Physics.

# A high-resolution integrated model of the National Ignition Campaign cryogenic layered experiments[a)]

O. S. Jones,[1,b)] C. J. Cerjan,[1] M. M. Marinak,[1] J. L. Milovich,[1] H. F. Robey,[1] P. T. Springer,[1] L. R. Benedetti,[1] D. L. Bleuel,[1] E. J. Bond,[1] D. K. Bradley,[1] D. A. Callahan,[1] J. A. Caggiano,[1] P. M. Celliers,[1] D. S. Clark,[1] S. M. Dixit,[1] T. Doppner,[1] R. J. Dylla-Spears,[1] E. G. Dzentitis,[1] D. R. Farley,[1] S. M. Glenn,[1] S. H. Glenzer,[1] S. W. Haan,[1] B. J. Haid,[1] C. A. Haynam,[1] D. G. Hicks,[1] B. J. Kozioziemski,[1] K. N. LaFortune,[1] O. L. Landen,[1] E. R. Mapoles,[1] A. J. MacKinnon,[1] J. M. McNaney,[1] N. B. Meezan,[1] P. A. Michel,[1] J. D. Moody,[1] M. J. Moran,[1] D. H. Munro,[1] M. V. Patel,[1] T. G. Parham,[1] J. D. Sater,[1] S. M. Sepke,[1] B. K. Spears,[1] R. P. J. Town,[1] S. V. Weber,[1] K. Widmann,[1] C. C. Widmayer,[1] E. A. Williams,[1] L. J. Atherton,[1] M. J. Edwards,[1] J. D. Lindl,[1] B. J. MacGowan,[1] L. J. Suter,[1] R. E. Olson,[2] H. W. Herrmann,[3] J. L. Kline,[3] G. A. Kyrala,[3] D. C. Wilson,[3] J. Frenje,[4] T. R. Boehly,[5] V. Glebov,[5] J. P. Knauer,[5] A. Nikroo,[6] H. Wilkens,[6] and J. D. Kilkenny[6]
[1]*Lawrence Livermore National Laboratory, 7000 East Avenue, L-399, Livermore, California 94551, USA*
[2]*Sandia National Laboratory, Albuquerque, New Mexico 87185, USA*
[3]*Los Alamos National Laboratory, Los Alamos, New Mexico 87545, USA*
[4]*Massachusetts Institute of Technology, Cambridge, Massachusetts 02139, USA*
[5]*Laboratory for Laser Energetics, Rochester, New York 14623, USA*
[6]*General Atomics, San Diego, California 92186, USA*

(Received 16 December 2011; accepted 23 April 2012; published online 29 May 2012)

A detailed simulation-based model of the June 2011 National Ignition Campaign cryogenic DT experiments is presented. The model is based on integrated hohlraum-capsule simulations that utilize the best available models for the hohlraum wall, ablator, and DT equations of state and opacities. The calculated radiation drive was adjusted by changing the input laser power to match the experimentally measured shock speeds, shock merger times, peak implosion velocity, and bangtime. The crossbeam energy transfer model was tuned to match the measured time-dependent symmetry. Mid-mode mix was included by directly modeling the ablator and ice surface perturbations up to mode 60. Simulated experimental values were extracted from the simulation and compared against the experiment. Although by design the model is able to reproduce the 1D in-flight implosion parameters and low-mode asymmetries, it is not able to accurately predict the measured and inferred stagnation properties and levels of mix. In particular, the measured yields were 15%–40% of the calculated yields, and the inferred stagnation pressure is about 3 times lower than simulated. © *2012 American Institute of Physics*. [http://dx.doi.org/10.1063/1.4718595]

## I. INTRODUCTION

The present indirect drive National Ignition Campaign (NIC) experiments use a laser-heated hohlraum that provides soft x-ray radiation drive to implode a spherical capsule containing a cryogenic DT fuel layer. The capsule needs to be imploded nearly symmetrically, with sufficient velocity, and with the fuel on a low adiabat in order to assemble a hotspot surrounded by cold, dense fuel that will ignite and burn.[1] The NIC strategy relies on a series of symmetry, shock timing, and ablator experiments to experimentally tune the implosion to the required velocity, symmetry, etc.[2–4]

We have modelled the DT implosions using the Hydra radiation hydrodynamics code.[5] The 2-D integrated (hohlraum + capsule) simulations described in this paper use the "high-flux model"—electron thermal conduction with a flux-limiter f = 0.15 and the direct configuration accounting (DCA) non-local thermodynamic equilibrium (nLTE) atomic physics model.[6] The hohlraum wall opacity is obtained from LTE tables (calculated offline using separate codes) for temperatures below 300 eV. Above 300 eV, the inline DCA model computes the non-LTE emissivity and opacity. Tabular opacities and equation of state are used for the ablator and DT fuel. The input laser sources are adjusted to account for the backscattered energy and the crossbeam energy transfer that occurs in the hohlraum plasma.[7,8] The Monte Carlo particle transport package was used to generate realistic neutron spectra for simulated neutron diagnostics.

We have found that when we apply the model described above to the shock timing[3] and convergent ablation[4] experiments, it overestimates the shock speeds and shell velocity, and as a result predicts x-ray bangtimes ~300–700 ps earlier than measured. Thus the simulations have a higher implosion velocity and a different fuel adiabat than the experiment, so the 1-D performance is quite different. This 1-D discrepancy makes it difficult to use these calculations to assess the 3-D degradation occurring in the experiment.

## II. DEVELOPMENT OF THE SEMI-EMPIRICAL MODEL

The goal of this work was to modify the integrated simulation model such that it better matches the available experimental

[a)]Paper KI3 1, Bull. Am. Phys. Soc. **56**, 180 (2011).
[b)]Invited speaker.

 

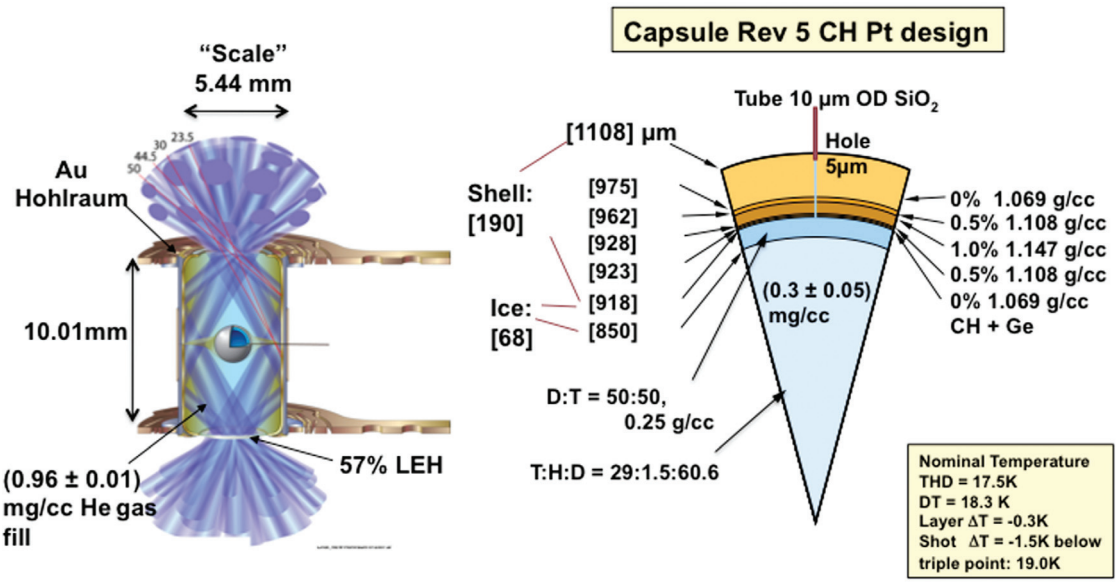


FIG. 1. Schematic of a cryogenic layered DT ignition target showing hohlraum and capsule dimensions.

data, and thus more accurately predicts the implosion dynamics and fuel assembly. An additional goal was to quantify to the extent to which the experimental performance differs from expectations based on our current physics models. The ignition threshold factor (ITF) performance metric[9] provides a useful framework for discussing the factors that determine the final state of the assembled fuel. The formula for ITF is

$$ITF = I_0\left(\frac{v}{v_0}\right)^8\left(\frac{\alpha}{\alpha_0}\right)^{-4}\left(1 - 1.2\frac{\Delta R^{K-wtd}_{hotspot}}{R_{hotspot}}\right)^4 \times \left(\frac{M_{clean}}{M_{DT}}\right)^{0.5}(1 - P_{HS}), \quad (1)$$

where $I_0$ is a constant, v is the peak fuel velocity ($v_o = 370$ km/s), $\alpha$ is the adiabat of the fuel at time of peak velocity ($\alpha_o = 1.4$), $\Delta R$ is the mode-number-weighted deviation of the hotspot from round, $M_{clean}/M_{DT}$ is the fraction of the initial cryogenic fuel mass that is not contaminated by mix, and $P_{HS}$ is a hotspot purity factor that is related to the amount of ablator material that is mixed deep into the hotspot.[9] This parameter defines a threshold for ignition. Implosions with an ITF of 1 +/− 0.15 have a 50% probability of igniting (yield > 1 MJ). Note that the ITF is especially sensitive to changes in velocity, adiabat, and hotspot shape.

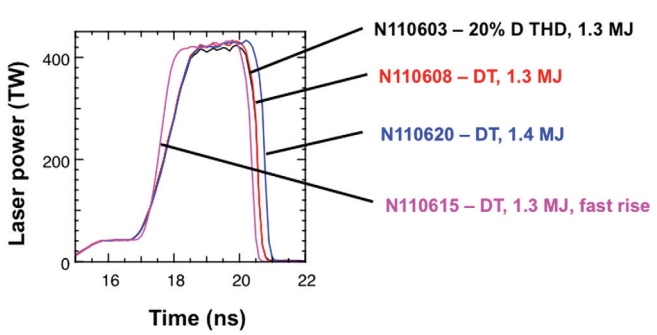


FIG. 2. Measured laser power during peak for the four cryogenic layered experiments that were simulated.

Ideally, we want a simulation model that accurately predicts the ITF that we infer from experimental data. While the terms in the ITF expression are not directly measurable, they are closely related to measured quanitites. The fuel adiabat is determined by the timing of the shocks that are driven by the multistep radiation drive.[1] The shock speeds and merger times are measured in liquid-deuterium-filled capsules using laser Doppler velocimetry.[3] The fuel velocity is closely related to the measured velocity of the imploding shell inferred from backlit implosions.[4] The low mode shape of the hotspot is inferred from gated, filtered (10 keV) x-ray images of the capsule self emission.[2] Higher mode distortions are not directly measurable, but can be included in calculations by applying realistic surface perturbations of the ablator and ice surfaces.

In this study, we focused on four cryogenic layered implosions from June, 2011. The nominal hohlraum and capsule dimensions for these experiments are shown in Fig. 1. These experiments used similar shock-timed, ~20 ns, 1.3–1.4 MJ shaped laser pulses with a peak power of 420 TW to heat a

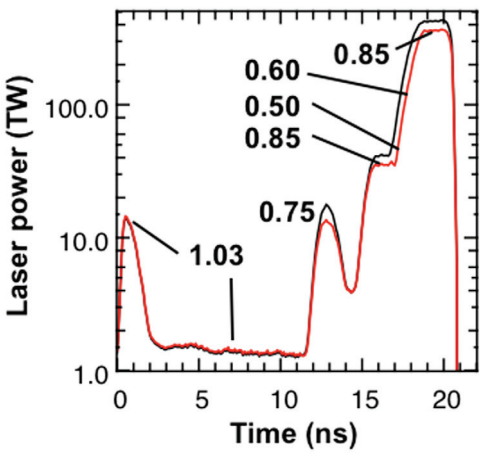


FIG. 3. Measured laser power (black) and input to simulation (red) after applying multipiers to match experimental data.

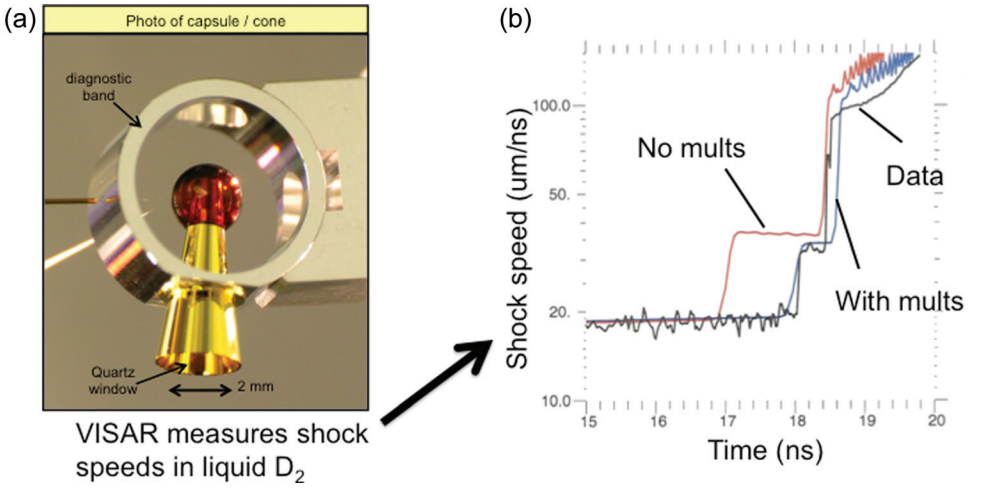


FIG. 4. (a) Partially assembled shock timing target. (b) Experimentally measured shock speed versus time (black) for N110521 shock timing experiment compared to simulation without laser power adjustment (red) and with adjustment (blue).

gold 5.44 mm diameter hohlraum and provide the soft x-ray drive to implode the capsules. The capsules consisted of a 190-$\mu$m-thick Ge-doped CH ablator surrounding a 68-$\mu$m-thick cryogenic DT fuel layer. The peak portion of the measured laser power is shown in Fig. 2 for these experiments. Shot N110603 had a THD (tritium-hydrogen-deuterium) fuel layer with 20% D fraction. Shot N110608 used the same laser pulse, but the capsule had a 50/50 DT fuel mixture. Shot N110620 was a 50/50 DT fuel layer, but the peak power was extended by 240 ps, increasing the laser energy from 1.3 to 1.4 MJ. N110615 was another 1.3 MJ DT shot, but with the rise time of the 4th pulse shortened. This set of four layered implosions had several tuning experiments associated with it. Three shock-timing experiments (N110517, N110519, and N110521) were done to measure the shock velocities, merger times, and merger depths,[3] and to adjust the laser pulse to get the desired ignition design values. The tuned pulse was then used in a convergent ablator experiment (N110625) in which the radius versus time of the converging shell was measured using time-dependent radiography.[4]

To create our semi-empirical calculation-based model, we simulated the tuning experiments with our standard Hydra model described previously and then adjusted the input laser power to best fit the data. The resulting laser power multipliers are shown in Fig. 3. Note that the strengths of the 2nd, 3rd, and 4th shocks had to be reduced substantially. Figure 4(a) shows a partially assembled shock timing target. The liquid deuterium-filled capsule has a re-entrant gold cone that allows the VISAR instrument to see inside the capsule and measure the speed of each shock as it breaks out of the inside of the ablator. Figure 4(b) shows the measured shock velocity versus time for the N110521 shock timing experiment. When the drive is not reduced (red curve), the simulated shock speeds are clearly higher than the measurement (black curve). The drive adjustment shown in Figure 3 brings the simulated speeds (blue curve) into better agreement. Thus, we expect that the adiabat calculated with the reduced drive should be in closer agreement with the actual adiabat.

Fig. 5 compares the measurements and simulations for the N110625 backlit implosion. We found that by multiplying

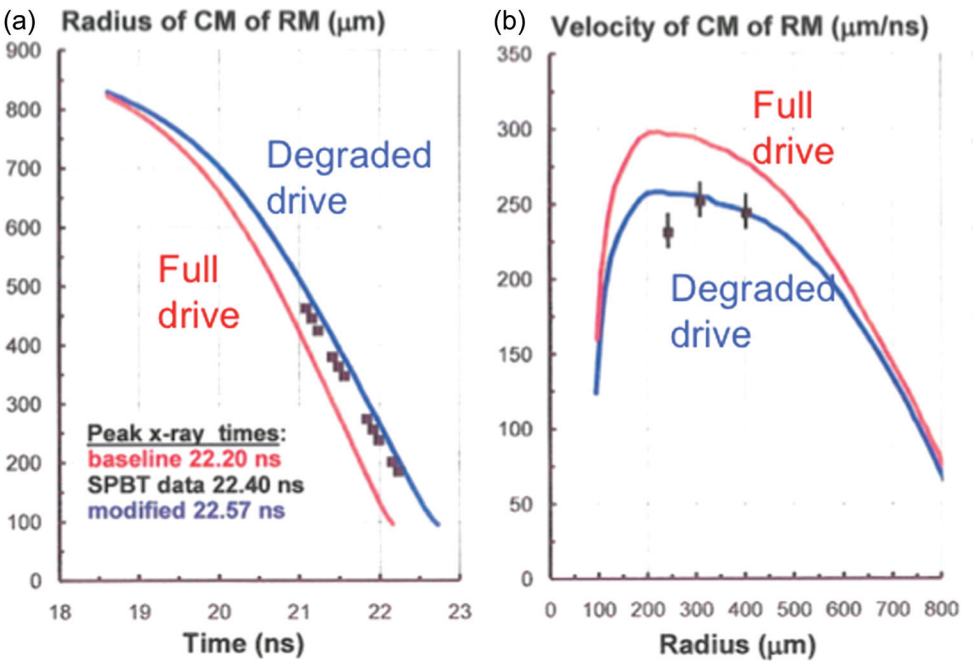


FIG. 5. (a) Plot of the center of mass of the remaining mass versus time for N110625 convergent ablator experiment. Black squares (data) are compared to simulations with (blue curve) and without (red curve) laser power adjustment. (b) Plot of center of mass velocity versus radius for same experiment.

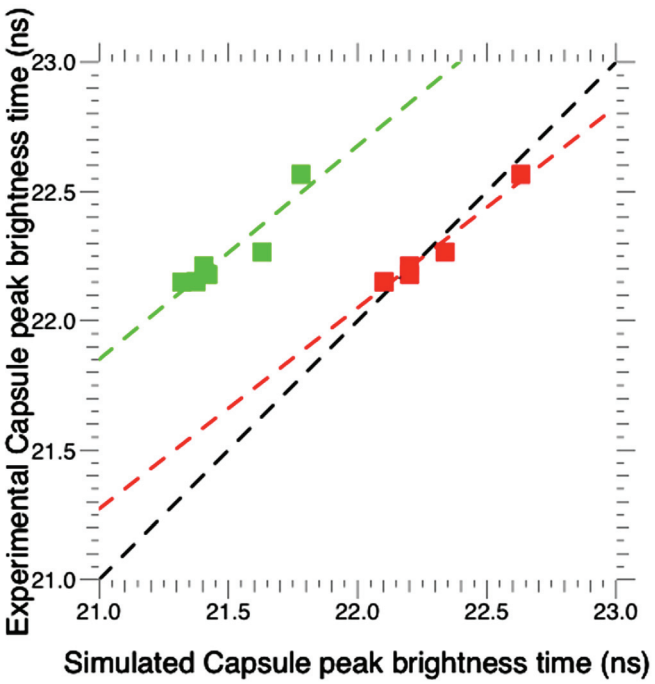


FIG. 6. Comparison of simulated and measured x-ray bangtime for simulations without multipliers (green) and with multipliers (red).

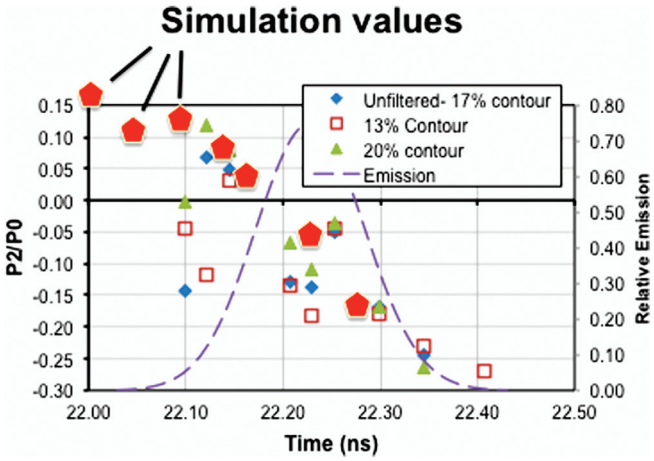


FIG. 8. Time dependence of the P2 Legendre moment of several contours of experimental gated x-ray image of shot N110620 compared to P2 moment of 17% contour of simulated x-ray images (red pentagons). Also shown is the emission versus time, indicating that peak emission (x-ray bangtime) occurs at 22.25 ns for this experiment.

the peak power by 0.85, we could bring the simulated shell trajectory and velocity into better agreement with the experiment. By lowering the simulated velocity, we also brought the simulated bangtimes into agreement with the measured bangtimes, as shown in Fig. 6. However, by significantly reducing the peak power in the simulations, we see that the agreement between the peak measured and simulated x-ray drive as inferred from the Dante x-ray diode array[10] has been lost, as shown in Fig. 7. The fact that the simulation with reduced drive does not agree with the Dante measurements could either mean that the relationship between flux viewed by the Dante instrument and the flux actually impinging on the capsule is different in the experiment than in the simulations, due to some kind of viewfactor effect, or that the coupling of the radiation drive onto the capsule is less efficient in the experiment due to some subtle ablation physics effects that are not included in our present models.

In addition to matching the velocity and adiabat, the semi-empirical model should also produce a realistic hotspot shape (the third term in ITF expression). The low mode shape (up to about Legendre mode 6) is largely determined by the radiation drive asymmetry. The smallest even Legendre mode, $P_2$, depends on the relative power between the inner cone beams (23.5° and 30°) that deliver power to the waist of the hohlraum and the outer cone beams (44.5° and 50°) that deliver power closer to the laser entrance hole (see Fig. 1). To obtain the correct ratio of inner cone power to total power, the input measured laser powers are modified by subtracting the measured backscattered power due to laser plasma instabilities and calculating the amount of power transfer between the beams as they cross at the laser entrance hole. Experimentally, the amount of power transferred between the inner and outer cones is controlled by changing the wavelength separation between the inner and outer cone beams.[8] The power transfer is calculated using a code that uses the calculated plasma conditions and the beam crossing geometry.[8] We can vary the amount of calculated power transfer by adjusting the $\delta n/n$ at which the transfer saturates, where n is the electron density in the beam crossing volume.

We adjusted the crossbeam model by calculating layered experiment N110620 with "clean" ablator and DT surface (no imposed surface roughness) and varying the $\delta n/n$ parameter until we matched the time-dependent P2 shape inferred from

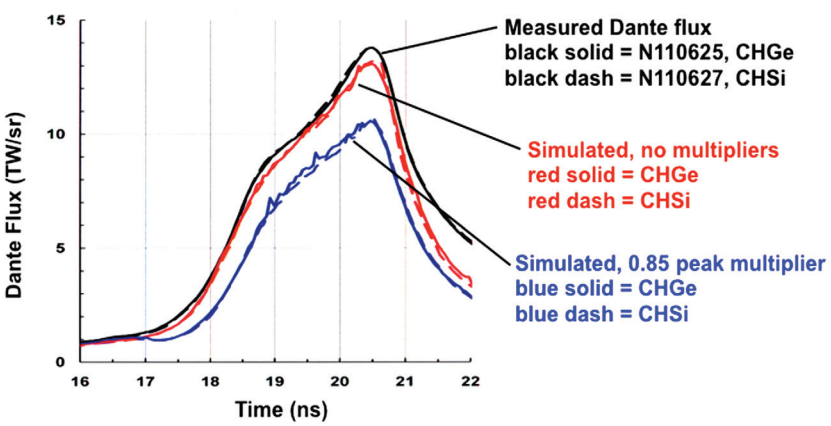


FIG. 7. Comparison of measured Dante flux versus time to simulated flux from simulation without multipliers (red) and with multipliers (blue).

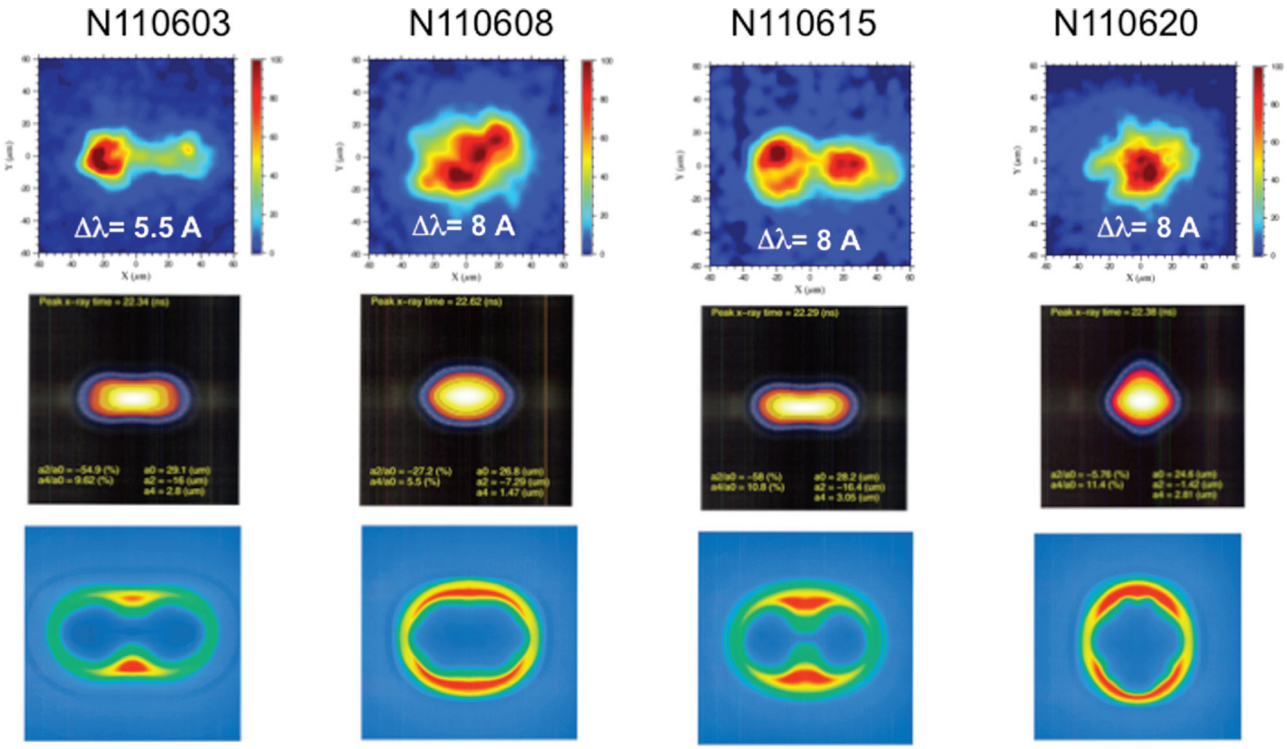


FIG. 9. Core symmetry at time of peak x-ray emission for the June 2011 layered experiments. First row are experiment gated x-ray images. Second row are simulated x-ray images. Third row are density contour plots at same times.

gated x-ray images of the core. Fig. 8 shows that the time-dependent symmetry agrees for a $\delta$n/n of 4 e-4. Using that same $\delta$n/n for all four layered simulations, we were able to match the experimental low mode shape, as shown in Fig. 9.

In addition to matching the low mode shape of the hotspot, we also included higher mode perturbations by putting realistic surface perturbations on all the ablator and DT ice surfaces (including all the internal interfaces). We applied perturbations at the NIF specification level[9] up to mode 60, with a random phase for each mode. The measured surfaces for these experiments were smoother than the specification, but the fill tube and grooves in the ice layer, which also perturb the hotspot[9] were not included. Not including the ice grooves is expected to have a small effect, since the ice layers for these shots had a total groove volume that met the NIC specification. We chose to include up to mode 60 because design calculations showed that the growth factor for capsules with a 190-$\mu$m-thick Ge-doped CH ablator peaks at about Legendre mode 60.[9] Note that the growth factor is defined as the ratio of the perturbation at the fuel-ablator interface at the time of peak velocity to the initial perturbation on the outside of the ablator. We have found that by including up to mode 60, we capture 70% of the rms perturbation at peak velocity and 95% of the rms perturbation of the final hotspot. Fig. 10 shows contour plots of the density and temperature of the hotspot near bangtime for the clean and mode 60 calculation of N110620. Significant perturbation

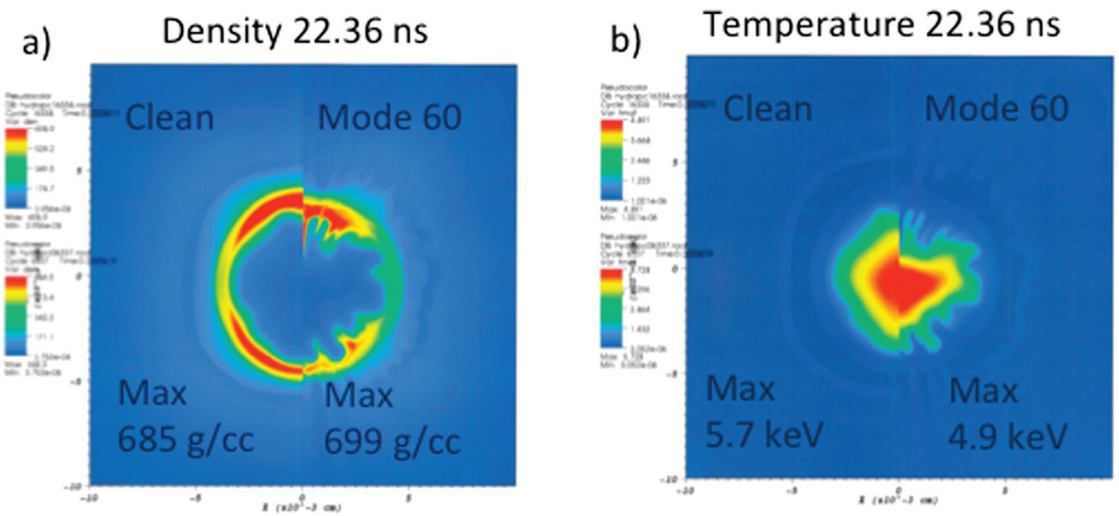


FIG. 10. Plots of (a) core density and (b) core temperature. Left side of plots is for calculation with smooth ablator and ice surfaces, while right side is for higher resolution calculation with imposed surface perturbations up to mode 60.

TABLE I. Summary of measured capsule performance metrics for experiment N110620 compared to simulated values from semi-empirical models of increasing complexity. YOS is measured yield over simulated yield.

| | N110620 experiment | 1D degraded drive | 2D match symmetry | 2D match symmetry + perturbations |
|---|---|---|---|---|
| Yield | 4.1e14 | 1.77e16 | 8.0e15 | 2.3e15 |
| YOS | — | 2.3% | 5.1% | 18% |
| Ti (keV) | 4.43 | 4.28 | 3.94 | 3.4 |
| DSR (%) | 4.5 | 6.4 | 6.3 | 5.6 |
| GBT (ns) | 22.31 | 22.44 | 22.44 | 22.41 |
| GBW (ps) | 175 | 76 | 102 | 112 |
| V(km/s) | — | 327 | 325 | 325 |
| Adiabat | — | 1.56 | 1.59 | 1.64 |

amplitudes are seen at the hotspot perimeter, which cool the hotspot compared to the clean calculations.

The final two terms in the ITF formula are due to high mode perturbations (up to about mode 2000) that mix ablator material into the fuel,[11] or, in the case of isolated defects on the ablator surface, can inject ablator material directly into the hotspot.[12] It is not practical to include these high mode perturbations in the integrated semi-empirical model. However, if the clean fuel fraction is about 78% as predicted for this ablator[11] and the amount of ablator mass is of order 30 ng,[12] then these terms have a minor impact on ITF compared with the velocity, adiabat, and hotspot shape terms that we have explicitly attemped to match in this model.

## III. COMPARISON OF THE SEMI-EMPIRICAL MODEL TO EXPERIMENTS

Table I compares measured capsule performance metrics with those extracted from simulations of increasing complexity for the N110620 DT experiment. The yield is the number of neutrons from DT fusion at 14.1 MeV integrated over the range from 13–15 MeV. The ion temperature is derived from the width of the neutron spectrum. The down-scattered ratio (DSR), which is defined as the ratio of the neutrons from 10–12 MeV to the neutrons from 13–15 MeV, is proportional to the areal density, $\rho$R, of the assembled fuel.[13] The gamma bang time (GBT) and burn width (GBW) extracted from the gamma reaction history (GRH) diagnostic[14] are also tabulated. The first column shows the experimental measurements. The second column shows the results for a calculation with the drive adjusted using the laser power multipliers and with the drive artificially symmetrized, so that the capsule is symmetrically imploded (quasi-1D calculation). The third column shows results for a calculation that also matches the low mode radiation symmetry, but has clean surfaces. The final column is the full semi-empirical model we have described, and so includes surface perturbations up to mode 60. The measured yield is substantially lower than the simulated yield, but the ratio of the yield over simulated (YOS) does increase to 18% for the full model. The calculated DSR and burn width get closer to the data for the full model, but the calculated ion temperature agreement gets slightly worse. The calculated velocity and adiabat are ~325 $\mu$m/ns and 1.6, respectively. The ideal design values are 370 $\mu$m/ns and 1.4.

Next, we compare capsule performance metrics for all four of the layered experiments we simulated with the model. Fig. 11 is a plot of calculated DSR, which is a

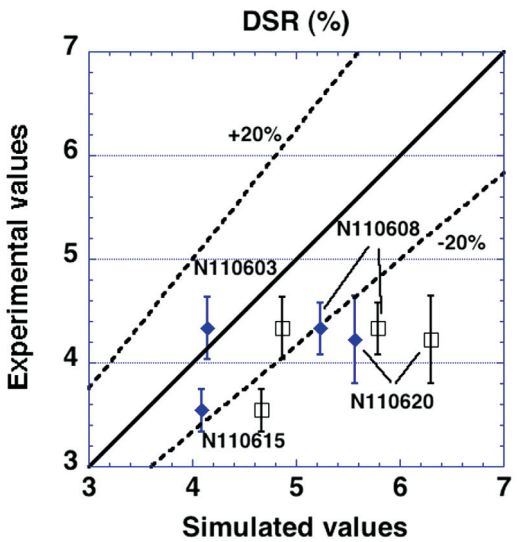


FIG. 11. Comparison of experimental and simulated neutron down scattered ratios. Open squares are simulations with clean surfaces and blue diamonds are simulations with mode 60 surface perturbations.

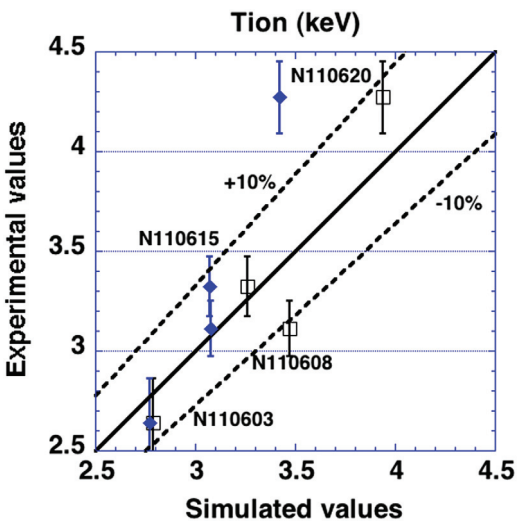


FIG. 12. Comparison of experimental and simulated burn-weighted ion temperatures. Open squares are simulations with clean surfaces and blue diamonds are simulations with mode 60 surface perturbations.

measure of the compression and $\rho$R, versus the measured values. The squares are the calculations that match the low mode symmetry and have clean surfaces. The diamonds are the results of the full semi-empirical model with mode 60 surface perturbations. With the exception of shot N110603, which was a highly distorted (pancaked) implosion, the simulations with mode 60 perturbations bring the simulated DSR closer to the data, although the experimentally measured DSR remains about 20% lower than the model predictions. Fig. 12 shows that the calculated ion temperatures are within 20% of the data, with the mode 60 calculations tending to slightly underestimate the temperature.

However, when we look at the burn, the agreement is not as good. Fig. 13 compares the calculated $\gamma$ burn width to that measured by the GRH. The experimentally measured burn width is consistently 50–100 ps (~40%) longer than calculated. Fig. 14 is a comparison of the calculated and measured neutron yield, where neutron yield here is defined as the neutrons with energies from 13–15 MeV. The calculated yield is consistently higher than the measured yield, with the YOS varying from 15%–40%. Note that the two experiments with the largest YOS are the two whose cores were most out of round, because the calculated yield was much less for those two experiments. The experimental yield appears to be much less sensitive to symmetry changes, which implies that something other than core symmetry is limiting the yield.

Thus, we see that although these simulations have been designed to roughly match the 1D inflight implosion parameters and low to mid mode asymmetry, the present model is not able to accurately predict the final stagnation conditions of the assembled fuel and hotspot. The present model tends to overestimate the compression and underestimate the yield and burn duration relative to the experimentally measured values. This is important because it quantifies the extent to which 3D high mode mix or other physics processes not included in the present model are reducing the capsule performance.

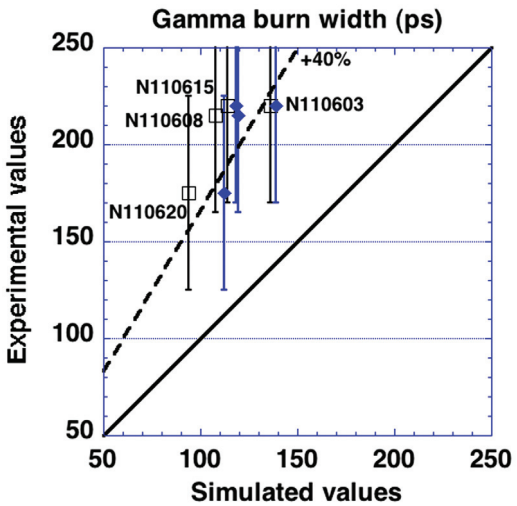


FIG. 13. Comparison of experimental and simulated gamma burn widths. Open squares are simulations with clean surfaces and blue diamonds are simulations with mode 60 surface perturbations.

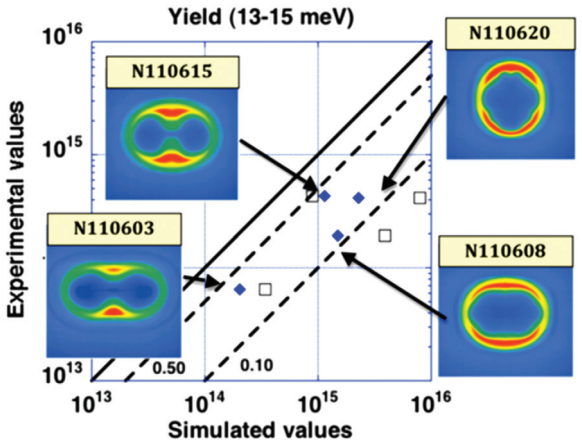


FIG. 14. Comparison of experimental and simulated neutron yields (neutrons from 13–15 MeV). Open squares are simulations with clean surfaces and blue diamonds are simulations with mode 60 surface perturbations.

## IV. COMPARISON TO A STATIC ISOBARIC HOTSPOT DATA-FITTING MODEL

To obtain further insight into the low experimental yields, we compared simulation results for N110620 to a static isobaric hotspot model fit to the experimental data.[15] To illustrate how the fitting model works, we express the yield as

$$Y \sim N_D N_T \langle \sigma v \rangle V \tau_b, \tag{2}$$

where $N_D$ and $N_T$ are the number densities of deuterium and tritium, $\langle \sigma v \rangle$ is the velocity-averaged reaction cross section, V is the hotspot volume, and $\tau_b$ is the burn duration. Notionally, the hotspot volume and burn duration come from the time-dependent x-ray image data, the yield and cross section come from the neutron data, and the number densities then are obtained from the fit. Using radiative, equation of state, nuclear fusion relations for relevant materials, and an approximation of pressure equilibrium within the hotspot,[16] the fitting model arrives at a 3-dimensional representation of the capsule density and temperature profiles at stagnation by predicting and optimizing fits to a broad set of x-ray and nuclear diagnostics. From the best-fit density and temperature profiles, we can then derive various hotspot quantities.

Table II shows the comparison of hotspot quantities from the static isobaric hotspot model fit and from the semi-empirical model described in this paper. The semi-empirical model has hotspot density about 4 times larger than the fit, a

TABLE II. Comparison between hotspot parameters inferred from static isobaric best fit model and same parameters extracted from 2D simulation for shot N110620.

| | Isobaric model best fit | 2D simulation | Sim/Fit |
|---|---|---|---|
| Yield (kJ) | 1.5 | 27 | 18 |
| Ti (keV) | 4.4 | 3.9 | 0.89 |
| X-ray a0 ($\mu$m) | 24 | 24 | 1 |
| Burn wt. density (g/cc) | 26 +/− 13 | 100 | ~4 |
| Hotspot mass ($\mu$g) | 2.8 +/− 1.4 | 24 | ~8 |
| Pressure (Gbar) | 80 +/− 40 | 270 | ~3 |

hotspot mass about 8 times larger, and a pressure about 3 times larger. We can use Eq. (2) along with fact that $\langle \sigma v \rangle$ varies as $T^{4.7}$ to find that the pressure should scale as

$$P \sim nT \sim \sqrt{\frac{Y}{V\tau_b}} \frac{1}{T^{1.35}}. \quad (3)$$

We see that the higher calculated yield, shorter burn duration, and slightly lower ion temperature all conspire to give the semi-empirical model a higher pressure than is inferred from the fit.

We speculate that the low apparent fuel mass could be caused by cold fuel mixing and cooling the outside of what would have been a much larger hotspot. So in experiment N110620, the x-ray image is actually showing the inner part of a larger, more poorly compressed hotspot than is inferred from the simulations. The relatively poor compression could be due to a higher inflight adiabat on the inner part of the fuel caused by an unintentionally launched 5th shock or some other physical process that heats the inner part of the fuel layer. Or the Atwood number at the fuel-ablator interface could be much more unstable than we calculate, which would also be consistent with poorer compression and reduced yield.

## V. SUMMARY AND CONCLUSIONS

We have shown how we developed a semi-empirical model of the NIC layered implosions based on the integrated capsule-hohlraum calculations using the Hydra code. By adjusting the input laser power, matching the experimental symmetry, and including realistic ablator and ice surface perturbations, we are able to approximately match the velocity, shock timing, and hotspot shape inferred from the experimental data for a series of cryogenically layered implosion experiments. We showed that by adjusting one parameter in the crossbeam transfer model, the $\delta n/n$ at which the transfer process saturates, the semi-empirical model is able to predict changes in low mode symmetry as a result of changes in pulse shape, capsule dimensions, and laser color separation. However, although the model was designed to accurately capture the conditions of the incoming ablator/fuel assembly prior to stagnation by approximately matching 1D inflight parameters and low mode shape, we found that the model could not accurately predict the final conditions of the stagnated core. For example, the measured yield is consistently lower than calculated (YOS from 15%–40%) and the inferred $\rho R$ is about 20% lower than calculated. By comparing our model to a static isobaric hotspot model fit to the data, we also found that the hotspot mass, density, and pressure in our calculation-based model were higher than the same quantities inferred from the fit. We, therefore, conclude that, although some aspects of the implosion dynamics are nearly reproduced by the integrated model, there remain significant differences in conditions obtained with our best integrated models and the fuel assembly in the experiment.

## ACKNOWLEDGMENTS

This work was performed under the auspices of the U.S. Department of Energy by the Lawrence Livermore National Laboratory under Contract W-7409-Eng-48.

[1]J. D. Lindl, *Inertial Confinement Fusion* (Springer, New York, NY, USA, 1998).
[2]O. L. Landen, M. J. Edwards, S. W. Haan *et al.*, Phys. Plasmas **18**, 051002 (2011).
[3]H. F. Robey, T. R. Boehly, R. E. Olson *et al.*, Phys. Plasmas **17**, 012703 (2010).
[4]D. G. Hicks. B. K. Spears, D. G. Braun *et al.*, Phys. Plasmas **17**, 102703 (2010).
[5]M. M. Marinak, G. D. Kerbel, N. A. Gentile *et al.*, Phys. Plasmas **8**, 2275 (2001).
[6]M. D. Rosen, H. A. Scott, D. E. Hinkel *et al.*, High Energy Density Phys. **7**, 180 (2011).
[7]R. P. J. Town, M. D. Rosen, P. A. Michel *et al.*, Phys. Plasmas **18**, 056302 (2011).
[8]P. Michel, S. H. Glenzer, L. Divol *et al.*, Phys. Plasmas **17**, 056305 (2010).
[9]S. W. Haan, J. D. Lindl, D. A. Callahan *et al.*, Phys. Plasmas **18**, 051001 (2011).
[10]H. N. Kornbluth and R. L. Kauffman, Rev. Sci. Instrum. **57**, 2179 (1986).
[11]D. S. Clark, S. W. Haan, A. W. Cook, M. J. Edwards, B. A. Hammel, J. M. Koning, and M. M. Marinak, Phys. Plasmas **18**, 082701 (2011).
[12]B. A. Hammel, S. W. Haan, D. S. Clark, M. J. Edwards, S. H. Langer, M. M. Marinak, M. V. Patel, J. D. Salmonson, and H. A. Scott, High Energy Density Phys. **6**, 171 (2010).
[13]M. J. Edwards *et al.*, Phys. Plasmas **18**, 051003 (2011).
[14]H. W. Hermann, N. Hoffman, D. C. Wilson, W. Stoeffl, L. Dauffy, Y. H. Kim, A. McEvoy, C. S. Young, J. M. Mack, C. J. Horsfield, M. Rubery, E. K. Miller, and Z. A. Ali, Rev. Sci. Instrum. **81**, 10D333 (2010).
[15]P. Springer and C. Cerjan, in *IFSA Proceedings* Bordeaux, France (2011).
[16]M. C. Hermann, M. Tabak, and J. D. Lindl, Nucl. Fusion **41**, 99 (2001).